

Cosmological Density Distribution Function from the Ellipsoidal Collapse Model in Real Space

Yasuhiro Ohta,¹ Issha Kayo,¹ and, Atsushi Taruya^{1,2}

ohta@utap.phys.s.u-tokyo.ac.jp, kayo@utap.phys.s.u-tokyo.ac.jp,
ataruya@utap.phys.s.u-tokyo.ac.jp

ABSTRACT

We calculate the one-point probability distribution function (PDF) for cosmic density δ in non-linear regime of the gravitational evolution. Under the local approximation that the evolution of cosmic fluid fields can be characterized by the Lagrangian local dynamics with finite degrees of freedom, the analytic expressions of PDF are derived taking account of the smoothing effect. The validity and the usefulness of the local approximation are then discussed comparing those results with N-body simulations in a Gaussian initial condition. Adopting the ellipsoidal collapse model (ECM) and the spherical collapse model (SCM) as Lagrangian local dynamics, we found that the PDFs from the local approximation excellently match the simulation results in the case of the cold dark matter initial spectrum. As for the scale-free initial spectra given by $P(k) \propto k^n$, N-body result suffers from spurious numerical effects, which prevent us to give a detailed comparison. Nevertheless, at the quality of N-body data, the model predictions based on the ECM and the SCM quantitatively agree with N-body results in cases with spectral index $n < 0$. For the index $n \geq 0$, choice of the Lagrangian local dynamics becomes crucial for an accurate prediction and a more delicate modeling is required, however, we find that the model prediction based on the ECM provides a better approximation to the N-body results of cumulants and PDFs.

Subject headings: cosmology:theory — dark matter — galaxies:clusters:general — large scale structure of universe — methods:analytical

¹Department of Physics, School of Science, University of Tokyo, Tokyo 113, Japan.

²Research Center for the Early Universe(RESCEU), School of Science, University of Tokyo, Tokyo 113, Japan.

1. Introduction

The probability distribution function (PDF) of the cosmological density fluctuation is a fundamental statistical quantity characterizing the large-scale structure of the universe. In a standard picture of cosmic structure formation based on the cold dark matter scenario, the gravitational evolution of the dark matter distribution plays an essential role for the hierarchical nature of observed luminous distributions. Usually, the evolution of dark matter distribution is believed to be developed from a small initial fluctuation with Gaussian random distribution. While the PDF of density fluctuation retains Gaussian shape in a linear regime, the deviation from Gaussian distribution becomes significant in the non-linear regime of gravitational evolution.

A number of studies in quantifying the non-Gaussian properties of density field have been developed theoretically and observationally. From the numerical and the observational study, a systematic analysis using the cosmological N-body simulation or the observed galaxy distribution yield various phenomenological prescription for the density PDF in the non-linear regime (e.g., Saslaw & Hamilton 1984; Hamilton 1985; Gaztañaga & Yokoyama 1993; Ueda & Yokoyama 1996). Among them, the lognormal distribution has been long known to fit to the simulations quite accurately (e.g., Coles & Jones 1991; Coles, Melott, & Shandarin 1993; Bernardeau & Kofman 1995; Taylor & Watts 2000). Recently, Kayo, Taruya & Suto (2001) critically examined this issue using the high resolution N-body simulation with Gaussian initial conditions, and found that the accuracy of the lognormal model remains valid, irrespective of the nature of initial spectra. The weak dependence of the initial spectra was later investigated using the phenomenological models with dark halo approach (Taruya, Hamana & Kayo 2003).

On the other hand, from the analytical study, a perturbative construction of the PDFs has been exploited by Bernardeau (1992, 1994a) employing a field-theoretical approach and the predictions including the smoothing effect excellently match the N-body simulations in the weakly non-linear regime. Beyond the perturbative prediction, however, no exact treatment is present and the non-perturbative approximation or the phenomenological approach taking account of the empirical simulation results are necessary. Fosalba & Gaztañaga (1998a) and Scherrer & Gaztañaga (2001) proposed to use a spherical collapse model as a non-perturbative approximation to predict the higher-order moments and PDFs. In their treatment, one assumes that the Lagrangian dynamics of the local density field is simply described by spherical collapse model. Although this approximation clearly misses the non-locality of the gravity in the sense that the evolution of the local density field can be determined by the one-to-one local mapping, the advantage of this treatment is that one can easily calculate the higher-order correction of the moments and PDFs. Further, it turns

out that the spherical collapse approximation exactly recovers the leading order results of perturbation theory.

Recently, we generalize the idea of spherical collapse approximation to the local approximation in which the evolution of local density field is characterized by the Lagrangian local dynamics with finite degrees of freedom (Ohta, Kayo & Taruya 2003). As a demonstration, the PDFs were computed using the ellipsoidal collapse model. In the ellipsoidal collapse model, the local density at a position is expressed as the multivariate function of initial parameters, i.e., the principal axes of the ellipsoid given at the same position. Thus, the relation between the initial and evolved density field cannot be described by the one-to-one local mapping. As a consequence, the local approximation with ellipsoidal collapse model successfully explains the stochastic nature seen in the simulation, i.e., the joint probability between the initial and the evolved density fields, as has been reported by Kayo, Taruya & Suto (2001). In addition, the leading-order results from the ellipsoidal collapse model correctly reproduce those obtained from the exact perturbation theory.

In the present paper, we extend the previous study to the quantitative comparison between the local approximation and the N-body simulations. Evaluating the PDF of local density fields taking account of the smoothing effect, we consider the validity and the limitation of the local approximation with spherical and ellipsoidal collapse models. The PDFs from the spherical collapse model were previously compared with the N-body simulations in the case with cold dark matter (CDM) power spectrum (Scherrer & Gaztañaga 2001). In this paper, taking account of the smoothing effect, the N-body results with the scale-free initial spectra as well as the CDM spectrum are compared.

This paper is organized as follows. In section 2, we start to review the local approximation of one-point statistics developed by Ohta, Kayo & Taruya (2003) and briefly show how to compute the PDF and the moments from the Lagrangian local collapse model. As representative models of Lagrangian local dynamics, the spherical and the ellipsoidal collapse model are considered. Then, we consider the smoothing effect and discuss how to incorporate it into the model predictions. Based on this, the perturbative calculation of cumulants up to the two-loop order is presented and the qualitative behaviors of the model prediction are discussed in section 3. In section 4, the validity and the usefulness of the local approximation for one-point statistics is investigated by comparing the PDFs and cumulants from the local collapse models with those obtained from the N-body simulations. Finally, section 5 is devoted to discussion and conclusions.

2. One-point statistics from the local collapse model

In many analytical works on the gravitational evolution of density distributions, the cold dark matter distribution is often treated as the pressureless and non-relativistic fluid. This treatment is not exact, but in a statistical sense, it would provide a better approximation if the scale of our interest is large enough, where no shell-crossing appears in the smoothed density fields. Denoting the mass density and velocity field of fluid by ρ and \mathbf{v} , the evolution equations for the fluid in a homogeneous and isotropic background universe are expressed as follows:

$$\frac{\partial \delta}{\partial t} + \frac{1}{a} \nabla \cdot [(1 + \delta) \mathbf{v}] = 0, \quad (1)$$

$$\frac{\partial \mathbf{v}}{\partial t} + H \mathbf{v} + \frac{1}{a} (\mathbf{v} \cdot \nabla) \mathbf{v} = -\frac{1}{a} \nabla \phi, \quad (2)$$

where δ is the density fluctuation, $\delta \equiv (\rho - \rho_m)/\rho_m$. The quantity a is the scale factor of the universe and H is the Hubble parameter given by $H \equiv \dot{a}/a$. Gravitational potential ϕ is determined by the Poisson equation:

$$\nabla^2 \phi = 4\pi G \rho_m a^2 \delta. \quad (3)$$

Below, owing to the local approximation, we consider the one-point PDF of the density fluctuation δ and the higher-order moments taking account of the smoothing effect.

2.1. Local approximation

As mentioned in section 1, the analytical treatment of the one-point PDF $P(\delta)$ governed by the fluid equations (1)-(3) is generally intractable due to the non-linearity and the non-locality of the gravity. Beyond the perturbative prediction, a non-perturbative treatment should be exploited. The local approximation is one of the way to treat the one-point PDFs analytically by reducing the Lagrangian dynamics of the fluid motion given by (1)-(3) to the local dynamics with finite degrees of freedom. In this treatment, the time evolution of the local density field δ at a given position is determined by the local dynamics with the initial condition given at the same position in Lagrangian coordinate. Thus, the solution of local density field can be obtained by solving a couple of ordinary differential equation and expressed as a function of initial parameters $\boldsymbol{\lambda} = (\lambda_1, \lambda_2, \dots, \lambda_n)$ given at a Lagrangian position and time, i.e., $\delta = f(\boldsymbol{\lambda}, t)$. In this paper, we consider the spherical and the ellipsoidal collapse models as representative example of the Lagrangian local dynamics (see section 2.1.1 and 2.1.2). In this case, the initial parameters of Lagrangian local dynamics correspond to

the linearly extrapolated density fluctuation δ_l for the spherical collapse model and the principal axes of initial homogeneous ellipsoid, $(\lambda_1, \lambda_2, \lambda_3)$ for the ellipsoidal collapse model.

Once provided the functional form of the local density $f(\boldsymbol{\lambda}, t)$, the one-point PDF of the local density field $P(\delta; t)$ (in Eulerian space) can be analytically obtained. With a slight modification of the definition of density fluctuation δ so as to satisfy the normalization condition and the zero-mean of δ (Ohta, Kayo & Taruya 2003), one has

$$P(\delta, t) = \frac{1}{1 + \delta} \int \prod_{i=1}^n d\lambda_i P_i(\boldsymbol{\lambda}) \delta_D[\delta - g(\boldsymbol{\lambda}, t)], \quad (4)$$

where the function g is given by

$$\delta = g(\boldsymbol{\lambda}, t) \equiv N_E[1 + f(\boldsymbol{\lambda}, t)] - 1 \quad ; \quad N_E(t) \equiv \int \prod_{i=1}^n d\lambda_i \frac{P_i(\boldsymbol{\lambda})}{1 + f(\boldsymbol{\lambda}, t)}. \quad (5)$$

In equations (4) and (5), the function $P_i(\boldsymbol{\lambda})$ is the probability distribution of the initial parameters, which characterizes the randomness of the mass distribution. From (4), one also calculates the moments of the density fields:

$$\langle \delta^N \rangle \equiv \int \delta^N P(\delta, t) d\delta = \int \prod_{i=1}^n d\lambda_i \frac{g^N}{1 + g} P_i(\boldsymbol{\lambda}). \quad (6)$$

The expressions (4)-(6) are the heart of the analytical treatment in local approximation, which are rigorously derived by considering the evolution equations for the one-point PDFs (Ohta, Kayo & Taruya 2003).

2.1.1. Spherical collapse model

As simple Lagrangian local dynamics to calculate the function $f(\boldsymbol{\lambda}, t)$, let us first consider the spherical collapse model (SCM). In the SCM, the evolution of local density at a given position in Lagrangian space is determined by the mass M inside a sphere of radius R collapsing via self gravity:

$$\frac{d^2 R}{dt^2} = -\frac{GM}{R^2} + \frac{\Lambda}{3} R \quad ; \quad M = \frac{4\pi}{3} \bar{\rho} R^3 = \text{const}, \quad (7)$$

where Λ is cosmological constant. The above equation is re-expressed in terms of the local density defined by $\delta = (aR_0/R)^3 - 1$:

$$\frac{d^2 \delta}{dt^2} + 2H \frac{d\delta}{dt} - \frac{4}{3} \frac{1}{1 + \delta} \left(\frac{d\delta}{dt} \right)^2 = \frac{3}{2} H^2 \Omega_m (1 + \delta) \delta, \quad (8)$$

where Ω_m is the density parameter given by $\Omega_m \equiv 8\pi G\rho_m/(3H^2)$. Note that the SCM can be regarded as the monopole approximation of the fluid equations neglecting the shear and vorticity (e.g. Fosalba & Gaztañaga 1998a), since one obtains the following equation from (1)-(3) with a help of the Lagrangian time derivative, $d/dt \equiv \partial/\partial t + \mathbf{v}/a \cdot \nabla$:

$$\frac{d^2\delta}{dt^2} + 2H\frac{d\delta}{dt} - \frac{4}{3}\frac{1}{1+\delta}\left(\frac{d\delta}{dt}\right)^2 = H^2(1+\delta)\left(\frac{3}{2}\Omega_m\delta + \sigma^{ij}\sigma_{ij} - \omega^{ij}\omega_{ij}\right); \quad (9)$$

$$\sigma_{ij} = \frac{1}{2aH}\left(\frac{\partial v_i}{\partial x_j} + \frac{\partial v_j}{\partial x_i} - \frac{2}{3}\nabla \cdot \mathbf{v}\delta_{ij}\right), \quad (10)$$

$$\omega_{ij} = \frac{1}{2aH}\left(\frac{\partial v_i}{\partial x_j} - \frac{\partial v_j}{\partial x_i}\right), \quad (11)$$

where σ_{ij} and ω_{ij} respectively denote shear and vorticity tensor.

The exact solution of the equation (7) is obtained in the case of the Einstein-de Sitter universe ($\Omega_m = 1, \Lambda = 0$) and is expressed as the function of linearly extrapolated density fluctuation δ_l in parametric form:

$$\delta = \frac{9}{2}\frac{(\eta - \sin \eta)^2}{(1 - \cos \eta)^3} - 1, \quad \delta_l = \frac{3}{5}\left[\frac{3}{4}(\eta - \sin \eta)\right]^{2/3} \quad (12)$$

for $\delta_l > 0$, and

$$\delta = \frac{9}{2}\frac{(\sinh \eta - \eta)^2}{(\cosh \eta - 1)^3} - 1, \quad \delta_l = -\frac{3}{5}\left[\frac{3}{4}(\sinh \eta - \eta)\right]^{2/3} \quad (13)$$

for $\delta_l < 0$. The relation between δ and δ_l in the above equation is fairly accurate even in the non Einstein-de Sitter universe (e.g. Nakamura & Suto 1995; Fosalba & Gaztañaga 1998b). We will extensively use (12) and (13) for later analysis. Note that in computing the density PDF, the linearly extrapolated density δ_l should be regarded as initial parameter and is treated as a random variable. Assuming the Gaussian initial condition, we have

$$P_I(\delta_l) = \frac{1}{\sqrt{2\pi}\sigma_l}e^{-(\delta_l/\sigma_l)^2/2}, \quad (14)$$

where the variable σ_l is the rms fluctuation of linear density field, $\sigma_l = \langle \delta_l^2 \rangle^{1/2}$.

2.1.2. Ellipsoidal collapse model

The ellipsoidal collapse model (ECM) is an extension of the SCM taking account of the non-sphericity. In this model, the dynamics of the local density is described by the self-gravitating uniform density ellipsoid characterized by the half length of the principal axes α_i ($i = 1, 2, 3$).

The local density of ECM is given by

$$\delta = \frac{a^3}{\alpha_1 \alpha_2 \alpha_3} - 1. \quad (15)$$

According to Bond & Myers (1996), the evolution equations of half length of axes become

$$\frac{d^2}{dt^2} \alpha_i = \frac{\Lambda}{3} \alpha_i - 4\pi G \rho_m \alpha_i \left(\frac{1 + \delta}{3} + \frac{b_i}{2} \delta + \lambda_{\text{ext},i} \right), \quad (16)$$

$$b_i = \alpha_1 \alpha_2 \alpha_3 \int_0^\infty \frac{d\tau}{(\alpha_i^2 + \tau) \prod_j (\alpha_j^2 + \tau)^{1/2}} - \frac{2}{3}. \quad (17)$$

The quantity $\lambda_{\text{ext},i}$ mimics the effect of external tidal shear, which was introduced for the consistency with Zel'dovich approximation:

$$\lambda_{\text{ext},i} = \begin{cases} \lambda_i - \frac{\lambda_1 + \lambda_2 + \lambda_3}{3} & ; \text{linear external tide,} \\ \frac{5}{4} b_i & ; \text{non-linear external tide,} \end{cases} \quad (18)$$

where λ_i denotes the initial perturbation of principal axis and evolves as $\lambda_i(t) = D(t)\lambda_i(t_0)$ with the variable D being the linear growth rate. Note that the inclusion of the external tidal term is necessary to reproduce the Zel'dovich approximation when we linearize the evolution equations.¹ In this paper, both cases of the external tidal term are considered in order to reveal the model dependence of the prediction, but in comparing with N-body simulation, the ECM results with linear external tide is presented for brevity. In presence of the external tide, the initial condition is specified by the Zel'dovich approximation. Identifying the variables λ_i with the initial parameters of α_i , we have

$$\alpha_i(t_0) = a(t_0)[1 - \lambda_i(t_0)] \quad (19)$$

$$\frac{d}{dt} \alpha_i(t_0) = \dot{a}(t_0)[1 - \lambda_i(t_0)] - a(t_0)\dot{\lambda}_i(t_0). \quad (20)$$

Note that the initial parameters λ_i are related to the linearly extrapolated density fluctuation δ_l by $\delta_l = \lambda_1 + \lambda_2 + \lambda_3$. Hence, the parameters λ_i should be treated as the random variables. For the Gaussian initial condition, the distribution function of λ_i is analytically expressed as follows (Doroshkevich 1970):

$$P_l(\lambda_i) = \frac{675\sqrt{5}}{8\pi\sigma_l^6} \exp\left(-3\frac{I_1^2}{\sigma_l^2} + 15\frac{I_2}{2\sigma_l^2}\right) (\lambda_1 - \lambda_2)(\lambda_2 - \lambda_3)(\lambda_1 - \lambda_3), \quad (21)$$

¹If this term is dropped, a consistent calculation with initial distribution (21) is also impossible.

where we define $I_1 = \lambda_1 + \lambda_2 + \lambda_3$, $I_2 = \lambda_1\lambda_2 + \lambda_2\lambda_3 + \lambda_3\lambda_1$.

Note that in contrast to the SCM, the ECM can be regarded as an approximation of the fluid equations taking account of the effect of tidal shear but neglecting the vorticity (Ohta, Kayo & Taruya 2003). The equation (16) with (17) is re-expressed in terms of the local density δ (c.f., eq.[9]):

$$\frac{d^2\delta}{dt^2} + 2H\frac{d\delta}{dt} - \frac{4}{3}\frac{1}{1+\delta}\left(\frac{d\delta}{dt}\right)^2 = H^2(1+\delta)\left(\frac{3}{2}\Omega_m\delta + \sigma^{ij}\sigma_{ij}\right); \quad (22)$$

$$\sigma_{ij} = \frac{1}{3H}\left(3\frac{\dot{\alpha}_i}{\alpha_i} - \frac{\dot{\alpha}_1}{\alpha_1} - \frac{\dot{\alpha}_2}{\alpha_2} - \frac{\dot{\alpha}_3}{\alpha_3}\right)\delta_{ij}. \quad (23)$$

2.2. Smoothing effect

When we evaluate the statistical quantities from the N-body simulations, the smoothing procedure is often employed to remedy the discreteness of the particle data. In this sense, the smoothing effect is crucial and should be incorporated into the theoretical prediction. In this paper, we adopt the top-hat smoothing and the smoothed density PDFs are computed from both the local approximation and N-body simulation:

$$\hat{\delta}(\mathbf{x}; R) = \int d^3\mathbf{y} \delta(\mathbf{y}) W_{\text{TH}}(|\mathbf{y} - \mathbf{x}|; R); \quad (24)$$

$$W_{\text{TH}}(r; R) = \begin{cases} 3/4\pi R^3 & r < R \\ 0 & \text{otherwise} \end{cases}, \quad (25)$$

where $W_{\text{TH}}(r; R)$ is the top-hat smoothing kernel of the radius R .

A systematic method to compute the analytic PDFs taking account of the smoothing effect was first considered by Bernardeau (1994a) based on the perturbation theory. Later, his method was extended to the non-perturbative calculation of the PDF using SCM (Fosalba & Gaztañaga 1998a). We briefly review the method by Fosalba & Gaztañaga (1998a).

First notice the fact that in the case of the top-hat smoothing, the leading-order results of cumulants for local density field is not affected by the smoothing in Lagrangian space (Bernardeau 1994a). Extrapolating this result to the non-perturbative approximation with SCM, one can approximate the evolved local density with top-hat smoothing by

$$\hat{\delta} \approx f(\delta_{i,L}), \quad (26)$$

where $\hat{\delta}$ is the smoothed density and $\delta_{i,L}$ is the linear density fluctuation in Lagrangian space. To relate the quantity $\delta_{i,L}$ with that in Eulerian space, $\delta_{i,E}$, we recall the fact that the radius

R defined in the Eulerian space roughly corresponds to the radius $R(1 + \hat{\delta})^{1/3}$ in Lagrangian space. Thus, we have

$$\frac{\delta_{l,E}}{\sigma_l(R)} = \frac{\delta_{l,L}}{\sigma_l[R(1 + \hat{\delta})^{1/3}]} . \quad (27)$$

Substituting (27) into (26) and identifying the linear fluctuation $\delta_{l,E}$ with the smoothed linear fluctuation $\hat{\delta}_l$, the relation between $\hat{\delta}$ and $\hat{\delta}_l$ becomes

$$\hat{\delta} = \hat{f}(\hat{\delta}_l) \approx f \left\{ \frac{\sigma_l[R(1 + \hat{\delta})^{1/3}]}{\sigma_l(R)} \hat{\delta}_l \right\} . \quad (28)$$

The above relation can be further simplified by the running index γ defined by $\gamma \equiv d \log \sigma_l^2 / d \log R$:

$$\hat{f}(\hat{\delta}_l) = f \left\{ \left[1 + \hat{f}(\hat{\delta}_l) \right]^{\gamma/6} \hat{\delta}_l \right\} \quad ; \quad \gamma = \frac{d \log \sigma_l^2}{d \log R} = -(n + 3), \quad (29)$$

where n is the index of the initial power spectrum, $P(k) \propto k^n$. Notice that the above expression is still valid in the non power-law cases of the initial power spectrum. The remarkable feature in the relation (28) or (29) is that the leading order result of the cumulants obtained from the perturbation theory is exactly recovered by the local approximation with SCM.

Owing to this noticeable fact, we extend to use the result (29) to the local approximation with the ECM. In this case, the smoothed density field is related to the top-hat filtered principal axis $\hat{\lambda}_i$ given by:

$$\hat{f}(\hat{\boldsymbol{\lambda}}, t) = f \left\{ \left[1 + \hat{f}(\hat{\boldsymbol{\lambda}}, t) \right]^{\gamma/6} \hat{\boldsymbol{\lambda}}, t \right\} , \quad (30)$$

Adopting this form, the PDF (4) becomes

$$P(\hat{\delta}; R) = \frac{1}{1 + \hat{\delta}} \int \prod_{i=1}^3 d\hat{\lambda}_i P_I(\hat{\boldsymbol{\lambda}}) \delta_D \left[\hat{\delta} - \hat{g}(\hat{\boldsymbol{\lambda}}, t) \right] , \quad (31)$$

with $\hat{g}(\hat{\boldsymbol{\lambda}}, t)$ being

$$\hat{g}(\hat{\boldsymbol{\lambda}}, t) = \hat{N}_E \left[1 + \hat{f}(\hat{\boldsymbol{\lambda}}, t) \right] - 1 \quad ; \quad \hat{N}_E(t) = \int \prod_i d\hat{\lambda}_i \frac{P_I(\hat{\boldsymbol{\lambda}})}{1 + \hat{f}(\hat{\boldsymbol{\lambda}}, t)} . \quad (32)$$

The above equations apparently seem difficult to evaluate because of the implicit relation of the functions \hat{f} and $\hat{\boldsymbol{\lambda}}$. However, this apparent difficulty can be eliminated by introducing the following variables:

$$\lambda'_i = \left[1 + \hat{f}(\hat{\boldsymbol{\lambda}}, t) \right]^{\gamma/6} \hat{\lambda}_i . \quad (33)$$

Then the equation (31) becomes

$$P(\hat{\delta}; R) = \frac{1}{1 + \hat{\delta}} \int \prod_{i=1}^3 d\lambda'_i P_I \left\{ [1 + f(\boldsymbol{\lambda}', t)]^{-\gamma/6} \boldsymbol{\lambda}' \right\} \delta_D \left[\hat{\delta} - \hat{g}(\boldsymbol{\lambda}', t) \right] \left| \frac{\partial \hat{\lambda}_j}{\partial \lambda'_k} \right|, \quad (34)$$

where the quantities \hat{g} and \hat{N}_E can be recast as

$$\hat{g}(\boldsymbol{\lambda}', t) = \hat{N}_E [1 + f(\boldsymbol{\lambda}', t)] - 1 \quad ; \quad \hat{N}_E(t) = \int \prod_i d\lambda'_i \frac{P_I \left\{ [1 + f(\boldsymbol{\lambda}', t)]^{-\gamma/6} \boldsymbol{\lambda}' \right\}}{1 + f(\boldsymbol{\lambda}', t)} \left| \frac{\partial \hat{\lambda}_j}{\partial \lambda'_k} \right|. \quad (35)$$

Also, the Jacobian $|\partial \hat{\lambda}_j / \partial \lambda'_k|$ is calculated using the relation $\hat{\lambda}_i = [1 + f(\boldsymbol{\lambda}, t)]^{-\gamma/6} \lambda'_i$ as:

$$\left| \frac{\partial \hat{\lambda}_j}{\partial \lambda'_k} \right| = [1 + f(\boldsymbol{\lambda}', t)]^{-\gamma/2} \left(1 - \frac{\gamma}{6} \frac{1}{1 + f} \sum_{i=1}^3 \lambda'_i \frac{\partial f}{\partial \lambda'_i} \right). \quad (36)$$

Note that the term $-1/(1 + f) \sum_{i=1}^3 \lambda'_i (\partial f / \partial \lambda'_i)$ is related to the velocity divergence and is expressed as $\theta = \sum_i \dot{\alpha}_i / (H \alpha_i) - 3$ in the case of the Einstein-de Sitter universe. Thus, provided the solution of the equations for ECM (eqs.[15]-[17]), the smoothed density PDF can be numerically evaluated by substituting the solution $f(\boldsymbol{\lambda}, t)$ into the above equations. Similarly, the higher-order moments of the local density becomes

$$\langle \hat{\delta}^N \rangle = \int \hat{\delta}^N P(\hat{\delta}; R) d\delta = \int \prod_{i=1}^3 d\lambda'_i \frac{\hat{g}^N}{1 + \hat{g}} P_I \left[(1 + f)^{-\gamma/6} \boldsymbol{\lambda}' \right] \left| \frac{\partial \hat{\lambda}_j}{\partial \lambda'_k} \right|. \quad (37)$$

In what follows, we simply denote the smoothed density field $\hat{\delta}$ by δ .

3. Perturbation theory in Ellipsoidal Collapse Model

Before proceeding to compare the theoretical models with N-body simulations, it is useful to examine the perturbative analysis of the local collapse models. In this section, based on the ellipsoidal collapse model, we present the perturbative calculation of the cumulants of density field. The differences between the model predictions as well as the qualitative behaviors are also discussed in section 3.3.

Here and in what follows, we treat the evolution of local density in an Einstein-de Sitter universe. In this case, the linear growth rate D is simply proportional to the scale factor a . Let us denote the half-length of the principal axis α_i by

$$\alpha_i(t) = a(t) \{1 - \zeta_i(a(t))\}. \quad (38)$$

Then, regarding the scale factor a as time variable, the equation (16) is transformed to

$$a^2 \frac{d^2 \zeta_i}{da^2} + \frac{3}{2} a \frac{d\zeta_i}{da} = \frac{3}{2} (1 - \zeta_i) \left(\frac{1}{3} \delta + \frac{1}{2} b_i \delta + \lambda_{\text{ext},i} \right). \quad (39)$$

In terms of the variable ζ_i , the quantities b_i and δ are expressed as

$$b_i = (1 - \zeta_1)(1 - \zeta_2)(1 - \zeta_3) \int_0^\infty \frac{d\tau}{\{(1 - \zeta_i)^2 + \tau\} \prod_j \{(1 - \zeta_j)^2 + \tau\}^{1/2}} - \frac{2}{3} \quad (40)$$

$$\equiv \frac{4}{15} \{3\zeta_i - (\zeta_1 + \zeta_2 + \zeta_3)\} + \tilde{b}_i, \quad (41)$$

$$\delta \equiv \zeta_1 + \zeta_2 + \zeta_3 + \Delta. \quad (42)$$

Note that both of the quantities \tilde{b}_i and Δ are of the order of $\mathcal{O}(\zeta^2)$.

Below, we separately give the perturbation results in the ellipsoidal collapse model with non-linear external tide and with linear external tide. Note that the leading-order results for the cumulants in each model exactly coincide with each other and reproduce those of the exact perturbation theory (e.g., Bernardeau 1994a,b).

3.1. Ellipsoidal collapse model with non-linear external tide

In the case of the model with non-linear external tide, the quantity $\lambda_{\text{ext},i}$ is given by $(5/4)b_i$ and the right hand side of the equation (39) becomes $3\zeta_i/2 + \mathcal{O}(\zeta^2)$. Then We have

$$a^2 \frac{d^2 \zeta_i}{da^2} + \frac{3}{2} a \frac{d\zeta_i}{da} - \frac{3}{2} \zeta_i = \frac{1}{2} (\Delta - \delta \zeta_i) + \frac{3}{4} (1 - \zeta_i) b_i \delta + \frac{15}{8} (\tilde{b}_i - \zeta_i b_i) = \mathcal{O}(\zeta^2). \quad (43)$$

This equation can be perturbatively solved by substituting the series expansion $\zeta_i = \sum_{j=0} \xi_i^{(j)} a^j$ into the above equation. Under the initial condition (19), one formally obtains the expression of the coefficient $\xi_i^{(j)}$ as

$$\xi_i^{(1)} = \lambda_i(t_0) \quad (44)$$

$$\xi_i^{(j)} = \frac{1}{(2j+3)(j-1)j!} \frac{d^j}{da^j} \left[\Delta - \delta \zeta_i + \frac{3}{2} (1 - \zeta_i) b_i \delta + \frac{15}{4} (\tilde{b}_i - \zeta_i b_i) \right] \Big|_{a=0}; \quad j > 1, \quad (45)$$

where we have only considered the growing mode of the solutions. Note that the coefficient $\xi_i^{(j)}$ is the variable of the order of $\mathcal{O}(\lambda^j)$.

Based on the result (45), the perturbative expansion for the evolved density, $\delta = \sum_i \delta^{(i)}$, can be constructed from the relations (15), (38) and (40). The results up to the seventh

order become

$$\delta^{(1)} = \delta_l, \quad (46)$$

$$\delta^{(2)} = \frac{17}{21}\delta_l^2 + \frac{4}{21}J_1, \quad (47)$$

$$\delta^{(3)} = \frac{341}{567}\delta_l^3 + \frac{338}{945}\delta_l J_1 + \frac{92}{3969}J_2, \quad (48)$$

$$\delta^{(4)} = \frac{55805}{130977}\delta_l^4 + \frac{485288}{1091475}\delta_l^2 J_1 + \frac{234088}{4584195}\delta_l J_2 + \frac{429728}{10696455}J_1^2, \quad (49)$$

$$\begin{aligned} \delta^{(5)} = & \frac{213662}{729729}\delta_l^5 + \frac{292398464}{638512875}\delta_l^3 J_1 + \frac{64182728}{893918025}\delta_l^2 J_2 \\ & + \frac{6541246}{59594535}\delta_l J_1^2 + \frac{828974992}{96364363095}J_1 J_2, \end{aligned} \quad (50)$$

$$\begin{aligned} \delta^{(6)} = & \frac{21129781}{107270163}\delta_l^6 + \frac{15739030628}{37246584375}\delta_l^4 J_1 + \frac{38380501904}{469306963125}\delta_l^3 J_2 \\ & + \frac{334168450808}{1825082634375}\delta_l^2 J_1^2 + \frac{250313183728}{9368757523125}\delta_l J_1 J_2 \\ & + \frac{63778345006048}{7673012411439375}J_1^3 + \frac{2272657750768}{4603807446863625}J_2^2, \end{aligned} \quad (51)$$

$$\begin{aligned} \delta^{(7)} = & \frac{83411812}{639441621}\delta_l^7 + \frac{42267062029204}{116564878828125}\delta_l^5 J_1 + \frac{63224677073056}{769328200265625}\delta_l^4 J_2 \\ & + \frac{3019799334120902}{12565693937671875}\delta_l^3 J_1^2 + \frac{9581060236980928}{193511686640146875}\delta_l^2 J_1 J_2 \\ & + \frac{13515215809239748}{451527268827009375}\delta_l J_1^3 + \frac{276922264619192}{162549816777723375}\delta_l J_2^2 \\ & + \frac{9155185965341512}{3521912696850673125}J_1^2 J_2, \end{aligned} \quad (52)$$

where δ_l denotes the linear fluctuation given by $\delta_l = \lambda_1 + \lambda_2 + \lambda_3$. Here, we introduced the quantities $J_1 \equiv x^2 + xy + y^2$ and $J_2 \equiv (x - y)(2x + y)(x + 2y)$ with the variables x and y being $x = \lambda_1 - \lambda_2$ and $y = \lambda_2 - \lambda_3$, respectively.

Once provided the perturbative solution for the non-smoothed density field, cumulants for the smoothed density is calculated as follows. From the perturbative inversion of the relation (30), the smoothed density $\hat{\delta}$ is obtained and the normalization factor \hat{N}_E is first calculated by substituting this into the definition (32). Using the probability distribution of initial parameter (21), the resultant expression becomes

$$\begin{aligned} N_E = & 1 - \frac{1}{6}\gamma\sigma_l^2 + \left(\frac{10844}{848925} - \frac{79}{4410}\gamma - \frac{31}{378}\gamma^2 - \frac{1}{27}\gamma^3 \right) \sigma_l^4 \\ & + \left(\frac{3891599696}{511023137625} - \frac{1248901}{278107830}\gamma - \frac{47093}{415800}\gamma^2 \right. \\ & \left. - \frac{62341}{317520}\gamma^3 - \frac{19}{168}\gamma^4 - \frac{1}{48}\gamma^5 \right) \sigma_l^6 \end{aligned} \quad (53)$$

up to the order $\mathcal{O}(\sigma_l^6)$. Then, the moments for the smoothed density $\langle \hat{\delta}^N \rangle$ is evaluated from the relation $\langle \hat{\delta}^N \rangle = \int \prod_i d\lambda_i \hat{g}^N / (1 + \hat{g}) P_l(\boldsymbol{\lambda})$ (c.f. eq.[6]). Finally, the perturbative correction for the variance $\sigma^2 = \langle \hat{\delta}^2 \rangle$, the skewness $S_3 = \langle \hat{\delta}^3 \rangle / \sigma^4$ and the kurtosis $S_4 = (\langle \hat{\delta}^4 \rangle - 3\sigma^4) / \sigma^6$ are obtained and can be summarized as series expansion of σ_l^2 as follows:

$$\sigma^2 = \sigma_l^2 + s_{2,4} \sigma_l^4 + s_{2,6} \sigma_l^6 + s_{2,8} \sigma_l^8 + \dots, \quad (54)$$

$$S_3 = S_{3,0} + S_{3,2} \sigma_l^2 + S_{3,4} \sigma_l^4 + \dots, \quad (55)$$

$$S_4 = S_{4,0} + S_{4,2} \sigma_l^2 + S_{4,4} \sigma_l^4 + \dots. \quad (56)$$

The resultant expressions for the coefficients $s_{2,i}$, $S_{3,i}$ and $S_{4,i}$ become

$$s_{2,4} = \frac{439}{245} + \frac{167}{126} \gamma + \frac{11}{36} \gamma^2, \quad (57)$$

$$s_{2,6} = \frac{3143785639}{695269575} + \frac{15856223}{2037420} \gamma + \frac{55273}{10584} \gamma^2 + \frac{1835}{1134} \gamma^3 + \frac{127}{648} \gamma^4, \quad (58)$$

$$s_{2,8} = \frac{7932609222047169799}{537532462889296875} + \frac{2321384486861437}{54752479031250} \gamma + \frac{1062497682871}{20858087250} \gamma^2 + \frac{16268385923}{495093060} \gamma^3 + \frac{61875775}{5143824} \gamma^4 + \frac{13831}{5832} \gamma^5 + \frac{6877}{34992} \gamma^6 \quad (59)$$

for the variance,

$$S_{3,0} = \frac{34}{7} + \gamma, \quad (60)$$

$$S_{3,2} = \frac{1041064}{101871} + \frac{21946}{2205} \gamma + \frac{415}{126} \gamma^2 + \frac{10}{27} \gamma^3, \quad (61)$$

$$S_{3,4} = \frac{161751288183332}{3041804390625} + \frac{363349617641}{3476347875} \gamma + \frac{415283963}{5093550} \gamma^2 + \frac{11299781}{357210} \gamma^3 + \frac{2975}{486} \gamma^4 + \frac{1841}{3888} \gamma^5 \quad (62)$$

for the skewness and

$$S_{4,0} = \frac{60712}{1323} + \frac{62}{3} \gamma + \frac{7}{3} \gamma^2, \quad (63)$$

$$S_{4,2} = \frac{941370178286}{3476347875} + \frac{1518808496}{4584195} \gamma + \frac{18161033}{119070} \gamma^2 + \frac{3935}{126} \gamma^3 + \frac{1549}{648} \gamma^4, \quad (64)$$

$$S_{4,4} = \frac{30144942925392628918}{13782883663828125} + \frac{129392230965050887}{27376239515625} \gamma + \frac{397096017904379}{93861392625} \gamma^2 + \frac{30126971437}{15002820} \gamma^3 + \frac{1142621801}{2143260} \gamma^4 + \frac{6127195}{81648} \gamma^5 + \frac{102005}{23328} \gamma^6 \quad (65)$$

for the kurtosis.

3.2. Ellipsoidal collapse model with linear external tide

For the perturbative solution in the model with the linear external tide, the calculation is slightly reduced if we introduce the quantities $A = \zeta_1 + \zeta_2 + \zeta_3$, $B = \zeta_1 - \zeta_2$ and $C = \zeta_2 - \zeta_3$. Recalling the fact that the external tidal term becomes $\lambda_{\text{ext},i} = \lambda_i - (\lambda_1 + \lambda_2 + \lambda_3)/3$, the evolution equation (39) is rewritten with

$$a^2 \frac{d^2 A}{da^2} + \frac{3}{2} a \frac{dA}{da} - \frac{3}{2} A = \frac{3}{2} \Delta - \frac{1}{2} \delta A - \frac{3}{4} \sum_{i=1}^3 \zeta_i (\delta b_i + 2\lambda_{\text{ext},i}), \quad (66)$$

$$\begin{aligned} a^2 \frac{d^2 B}{da^2} + \frac{3}{2} a \frac{dB}{da} - \frac{3}{2} (\lambda_1 - \lambda_2) &= \frac{3}{4} \delta \{ (1 - \zeta_1) b_1 - (1 - \zeta_2) b_2 \} - \frac{1}{2} \delta B \\ &\quad - \frac{3}{2} (\zeta_1 \lambda_{\text{ext},1} - \zeta_2 \lambda_{\text{ext},2}), \end{aligned} \quad (67)$$

$$\begin{aligned} a^2 \frac{d^2 C}{da^2} + \frac{3}{2} a \frac{dC}{da} - \frac{3}{2} (\lambda_2 - \lambda_3) &= \frac{3}{4} \delta \{ (1 - \zeta_2) b_2 - (1 - \zeta_3) b_3 \} - \frac{1}{2} \delta C \\ &\quad - \frac{3}{2} (\zeta_2 \lambda_{\text{ext},2} - \zeta_3 \lambda_{\text{ext},3}). \end{aligned} \quad (68)$$

Note also that the right hand sides of the equation (66)-(68) are of the order of $\mathcal{O}(\lambda^2)$.

Similar to the procedure in section 3.1, the perturbative expansion for the density δ is constructed from the perturbative solutions of A , B and C . After a tedious but a straightforward calculation, the perturbative solutions up to the seventh order become

$$\delta^{(1)} = \delta_l, \quad (69)$$

$$\delta^{(2)} = \frac{17}{21} \delta_l^2 + \frac{4}{21} J_1, \quad (70)$$

$$\delta^{(3)} = \frac{341}{567} \delta_l^3 + \frac{1538}{4725} \delta_l J_1 + \frac{4}{405} J_2, \quad (71)$$

$$\delta^{(4)} = \frac{55805}{130977} \delta_l^4 + \frac{952144}{2480625} \delta_l^2 J_1 + \frac{345088}{16372125} \delta_l J_2 + \frac{12368}{363825} J_1^2, \quad (72)$$

$$\begin{aligned} \delta^{(5)} &= \frac{213662}{729729} \delta_l^5 + \frac{237342074}{621928125} \delta_l^3 J_1 + \frac{93363344}{3192564375} \delta_l^2 J_2 \\ &\quad + \frac{52865818}{638512875} \delta_l J_1^2 + \frac{135052}{34827975} J_1 J_2, \end{aligned} \quad (73)$$

$$\begin{aligned} \delta^{(6)} &= \frac{21129781}{107270163} \delta_l^6 + \frac{73816004896012}{215099024765625} \delta_l^4 J_1 + \frac{29134959410408}{879950555859375} \delta_l^3 J_2 \\ &\quad + \frac{45534497984}{355535578125} \delta_l^2 J_1^2 + \frac{1416570594232}{129059414859375} \delta_l J_1 J_2 \\ &\quad + \frac{797014912}{132368630625} J_1^3 + \frac{162352}{1578740625} J_2^2, \end{aligned} \quad (74)$$

$$\delta^{(7)} = \frac{83411812}{639441621} \delta_l^7 + \frac{24700151148166244}{85566392051765625} \delta_l^5 J_1$$

$$\begin{aligned}
& + \frac{49159400006961656}{1480956785511328125} \delta_l^4 J_2 + \frac{18569055254261594}{116681443706953125} \delta_l^3 J_1^2 \\
& + \frac{13101172588796}{684531136414125} \delta_l^2 J_1 J_2 + \frac{9323215177292}{488950811724375} \delta_l J_1^3 \\
& + \frac{1452480606736}{4400557305519375} \delta_l J_2^2 + \frac{11003633175272}{10267967046211875} J_1^2 J_2.
\end{aligned} \tag{75}$$

The normalization factor of the PDF is

$$\begin{aligned}
N_E = & 1 - \frac{1}{6} \gamma \sigma_l^2 + \left(\frac{69668}{3898125} + \frac{701}{198450} \gamma - \frac{31}{378} \gamma^2 - \frac{1}{27} \gamma^4 \right) \sigma_l^4 \\
& + \left(\frac{5033872069084}{645297074296875} + \frac{3873942169}{223479506250} \gamma - \frac{38616157}{509355000} \gamma^2 \right. \\
& \left. - \frac{286169}{1587600} \gamma^3 - \frac{19}{168} \gamma^4 - \frac{1}{48} \gamma^5 \right) \sigma_l^6.
\end{aligned} \tag{76}$$

Then, the coefficients of the perturbative correction for cumulants become

$$s_{2,4} = \frac{57137}{33075} + \frac{167}{126} \gamma + \frac{11}{36} \gamma^2, \tag{77}$$

$$s_{2,6} = \frac{469828713881}{111739753125} + \frac{17130160379}{2292097500} \gamma + \frac{488945}{95256} \gamma^2 + \frac{1835}{1134} \gamma^3 + \frac{127}{648} \gamma^4, \tag{78}$$

$$\begin{aligned}
s_{2,8} = & \frac{996244294855051546571}{74870593045294921875} + \frac{152613969392185373}{3871782445781250} \gamma + \frac{683964582869801}{14079208893750} \gamma^2 \\
& + \frac{1980638022487}{61886632500} \gamma^3 + \frac{306289019}{25719120} \gamma^4 + \frac{13831}{5832} \gamma^5 + \frac{6877}{34992} \gamma^6
\end{aligned} \tag{79}$$

for the variance,

$$S_{3,0} = \frac{34}{7} + \gamma, \tag{80}$$

$$S_{3,2} = \frac{646404856}{63669375} + \frac{327062}{33075} \gamma + \frac{415}{126} \gamma^2 + \frac{10}{27} \gamma^3, \tag{81}$$

$$\begin{aligned}
S_{3,4} = & \frac{77881923244216108}{1505693173359375} + \frac{80186055186641}{782178271875} \gamma + \frac{2052918391}{25467750} \gamma^2 \\
& + \frac{56239289}{1786050} \gamma^3 + \frac{2975}{486} \gamma^4 + \frac{1841}{3888} \gamma^5
\end{aligned} \tag{82}$$

for the skewness and

$$S_{4,0} = \frac{60712}{1323} + \frac{62}{3} \gamma + \frac{7}{3} \gamma^2, \tag{83}$$

$$S_{4,2} = \frac{210688932175742}{782178271875} + \frac{188859083824}{573024375} \gamma + \frac{90600877}{595350} \gamma^2 + \frac{3935}{126} \gamma^3 + \frac{1549}{648} \gamma^4, \tag{84}$$

$$\begin{aligned}
S_{4,4} = & \frac{102133149992759420855618}{47644922847005859375} + \frac{7007053550215029257}{1505693173359375} \gamma \\
& + \frac{29469590927547677}{7039604446875} \gamma^2 + \frac{13726819977457}{6876292500} \gamma^3 \\
& + \frac{5700735749}{10716300} \gamma^4 + \frac{6127195}{81648} \gamma^5 + \frac{102005}{23328} \gamma^6
\end{aligned} \tag{85}$$

for the kurtosis.

3.3. Differences between model predictions

To understand both the qualitative and the quantitative behaviors of the above two predictions, we here briefly discuss the systematic dependence of the perturbative results. Table 1 summarizes the numerical values of the coefficients, $s_{2,i}$ up to the three-loop order, and $S_{3,i}$ and $S_{4,i}$ up to the two-loop order for each model with various spectral indices. And using these results, we plot the cumulants up to the two-loop order in figure 1, where the cumulants are normalized by the leading-order results σ_l^2 , $S_{3,0}$ and $S_{4,0}$ (from *top* to *bottom*) and are depicted as function of linear variance σ_l . The results from the SCM (*short-dashed*) are essentially the same results as those obtained by Fosalba & Gaztañaga (1998a). Note that the leading-order results for the cumulants in all model predictions rigorously coincide with those obtained from the exact perturbation theory (e.g., Bernardeau 1994b), irrespective of the choice of the external tidal term.

Figure 1 shows that the differences between the model predictions are generally small for the spectral indices $n < 0$ and these are expected to become negligible as decreasing n , approaching the non-smoothing results ($n = -3$) as obtained previously (Ohta, Kayo & Taruya 2003). For $n = -2$, the predictions up to the one-loop order give

$$\sigma^2 \approx \sigma_l^2 + 0.61\sigma_l^4 \tag{86}$$

$$S_3 \approx 3.86 + 3.21\sigma_l^2 \tag{87}$$

for the SCM (Fosalba & Gaztañaga 1998a) and

$$\sigma^2 \approx \sigma_l^2 + 0.88\sigma_l^4 \tag{88}$$

$$S_3 \approx 3.86 + 3.18\sigma_l^2 \tag{89}$$

for the exact perturbation theory (Scoccimarro & Frieman 1996; Scoccimarro 1997). Comparing the above results with Table 1, the numerical values of the coefficients are close to those from the ECM prediction. On the other hand, for the $n = 0$ case, a large discrepancy appears in the variance σ^2 (Fig.1). The skewness and the kurtosis also show a relatively large difference. These behaviors are indeed consistent with the PDF shown in figure 5. The reason why the discrepancy in the model predictions become large as increasing n is partially ascribed to the Jacobian in the smoothed density PDF (34). The expression of the Jacobian $|\partial\hat{\lambda}_j/\partial\lambda'_k|$ in (36) contains the quantity related to the velocity divergence θ multiplied by the spectral dependent factor, $\gamma/6$. In previous study of the non-smoothing case (Ohta, Kayo & Taruya 2003), we found that while the differences between the model predictions are almost

negligible for the density fields, a large difference appears in the velocity divergence θ . This readily implies that the differences between the model predictions also become significant in the present case, depending on the factor $\gamma = -(n+3)$. In other words, for a large deviation from $\gamma = 0$, the model predictions sensitively depend on the choice of the Lagrangian local dynamics in local approximation. That is, not only the evolution of local density but also the evolution of velocity field should be devised to approximate the fluid dynamics precisely. This point is important and should be kept in mind when comparing the prediction with N-body simulations (see Sec.4.2).

4. Comparison with N-body simulations

We are now in position to discuss the validity and the usefulness of the local approximations comparing the theoretical prediction with N-body simulations. For this purpose, we specifically use the N-body data for the scale-free models with initial power spectra $P(k) \propto k^n$ ($n = -2, -1, 0$) (Jing 1998), as well as the CDM model with cosmological constant (Λ CDM; Jing & Suto 1998). The gravitational force calculation is based on the P³M algorithm. All the models employ $N = 256^3$ dark matter particles in a periodic comoving cube L_{BOX}^3 , where the box size of the Λ CDM model is chosen as $L_{\text{BOX}} = 300h^{-1}\text{Mpc}$. While the scale-free models assume an Einstein-de Sitter universe, cosmological parameters of the Λ CDM model are set as $(\Omega_m, \Omega_\Lambda, h, \sigma_8) = (0.3, 0.7, 0.7, 1.0)$, where the normalization σ_8 means the linear rms fluctuation at top-hat smoothing radius $R = 8h^{-1}\text{Mpc}$. For the scale-free models, the normalization of the density fluctuation is determined by setting the linear rms fluctuation to unity at $R = 0.1L_{\text{BOX}}$. Below, we first present the results in Λ CDM model (Sec.4.1). The PDFs in the scale-free models are compared in section 4.2. In comparing the prediction with simulation, we also present the perturbation results of local approximation obtained in previous section.

4.1. Λ CDM model

The validity of the local approximation using the SCM has been previously studied by Scherrer & Gaztañaga (2001) in the case of the standard CDM model and a good agreement with N-body simulation was found. We thus expect that the local approximation with both the SCM and the ECM also provides an excellent agreement with N-body simulation in the case of the Λ CDM model.

Figure 2 shows the PDFs obtained from the N-body data for the top-hat smoothed

density fields (*open-squares*). The error bars indicate the 1σ errors among three different realizations. The smoothing radii are chosen as $R = 16, 8, 2h^{-1}\text{Mpc}$ (from *top* to *bottom*). In figure 2, the PDFs from the SCM and the ECM with linear external tide are depicted as *long-dashed* and *solid* lines, respectively. We also calculated the PDFs from the ECM with non-linear external tide, but the results are almost the same as obtained from the ECM with linear external tide. Clearly, these models almost coincide with each other and the agreement with N-body results is excellently good. For comparison, we also plot the empirical model of the lognormal distribution (*short-dashed*):

$$P(\delta) = \frac{1}{\sqrt{2\pi}\sigma_{\text{LN}}} \frac{1}{1+\delta} \exp \left[-\frac{1}{2\sigma_{\text{LN}}^2} \left(\log(1+\delta) + \frac{\sigma_{\text{LN}}^2}{2} \right)^2 \right] \quad (90)$$

with $\sigma_{\text{LN}}^2 = \log(1 + \sigma^2)$. Here the quantity σ denotes the variance of the local density field, which is estimated from the N-body simulation. Albeit the simplicity of the analytical expression (90), the lognormal PDFs also approximate the N-body results quite accurately. Agreement with N-body simulation still remains good even at the high-density tails of small radii, $R = 2$ and $8h^{-1}\text{Mpc}$. Bernardeau & Kofman (1995) discuss the successful lognormal fit of the PDF in the CDM models based on the perturbation results.

In order to check the accuracy of the model predictions, we quantify the cumulants of the density fields. In figure 3, we plot the variance σ^2 , the skewness $S_3 \equiv \langle \delta^3 \rangle / \sigma^4$ and the kurtosis $S_4 \equiv (\langle \delta^4 \rangle - 3\sigma^4) / \sigma^6$ as a function of smoothing radius (from *top* to *bottom*). In each panel, the *crosses* with error bars indicate the results obtained from the N-body simulations, while the *open-squares* show the results from the local approximation with ECM, in which the moments $\langle \delta^N \rangle$ are calculated from the full knowledge of the PDF $P(\delta)$ (see eq.[37]). On the other hand, the short-dashed and the long-dashed lines are the perturbative calculations of the cumulants based on the ECM up to the one-loop order and the two-loop order, respectively(see Sec.3.2). As a reference, we also plot the leading-order(tree-level) prediction in dotted lines. In contrast to a naive expectation from figure 2, the ECM prediction based on the PDF significantly deviates from the N-body results at the smaller radius, $R \lesssim 8h^{-1}\text{Mpc}$, although it roughly match the perturbation results up to the two-loop order.

Kayo, Taruya & Suto (2001) remarked that the origin of this discrepancy might be due to the fact that the density field δ in N-body simulation does not extend the entire range between -1 and $+\infty$, but rather is limited in the range, $\delta_{\text{min}} < \delta < \delta_{\text{max}}$ owing to the finite size of the simulation box. Indeed, a closer look at figure 2 reveals that there exist the sharp cutoff at the high-density tails of simulated PDF(*arrows* in each panel). To examine the significance of this effect, the ECM predictions of the cumulants taking account of the finite range $[\delta_{\text{min}}, \delta_{\text{max}}]$ are plotted in figure 3 (cutoff-1, *open-triangles*). The cutoff values δ_{min} and δ_{max} are estimated from the N-body data. Further, in figure 3, we plot the prediction taking

account of the cutoff values determined from the simple assumptions that (i) the major effect for the finite range of δ comes from the finite sampling effect and (ii) the theoretical PDF is correct if the box size of the simulation becomes infinite. We then have (Kayo, Taruya & Suto 2001):

$$\frac{L_{\text{BOX}}^3}{4\pi R^3/3} \int_{-1}^{\delta_{\text{min}}} P(\delta)d\delta = 1, \quad \frac{L_{\text{BOX}}^3}{4\pi R^3/3} \int_{\delta_{\text{max}}}^{\infty} P(\delta)d\delta = 1, \quad (91)$$

where $P(\delta)$ is the PDF obtained from the ECM. The resultant cutoff values ($\delta_{\text{min}}, \delta_{\text{max}}$) are plotted as function of smoothing radii in figure 4.

The resultant amplitudes of the cumulants are significantly reduced and the model prediction turns out to reproduce the simulation data very well in the case using the N-body data (cutoff-1). This readily implies that the apparent discrepancy in the cumulants mainly comes from the limited range of the density in PDF and one concludes that the local approximation with ECM provides an accurate prediction for both the density PDF and the cumulants in the Λ CDM model. Similarly, one expects that the accuracy of the model prediction still remains good for the local approximation with SCM. Note, however, that the predictions with (91) still exhibits the discrepancy at the smaller scales $R \lesssim 4h^{-1}\text{Mpc}$. This means that the finite sampling effect might be a major numerical effect for the limited range of the density, but still not enough. The discreteness effect could be an important source for causing the discrepancy on small scales. This point is particularly important for self-consistent calculation of cumulants and should be treated carefully. Keeping these remarks in mind, we next proceed to the scale-free models.

4.2. Scale-free models

N-body simulations in scale-free model with index $n \leq -1$ generally suffer from spurious numerical effects compared to the CDM case, which significantly affects the statistical properties of mass distribution (e.g., Colombi, Bouchet & Hernquist 1996). This is not exceptional in our case. Figure 5 shows the density PDFs for $n = -2$ to 0 models at different smoothing radii; $R = 0.15, 0.1$ and $0.02L_{\text{BOX}}$. For larger smoothing radii, the PDF obtained from the simulations (*open-squares*) has a sharp cutoff at high-density tails. Because of this, the amplitude of the cumulants is significantly reduced and the N-body simulation fails to even reproduce the leading-order results of perturbation theory (see Figs.6 and 7). Nevertheless, focusing on the moderately non-Gaussian tails of PDF, we find that the predictions based on the SCM and ECM shows a good agreement with N-body simulations for smaller spectral indices, $n = -2, -1$. Especially at the non-linear scale ($R = 0.02L_{\text{BOX}}$), the PDF from the ECM seems to improve the prediction, compared to the results obtained from the

SCM. This is even true for the spectral index $n = 0$, indicating that the ECM provide a more physical model of Lagrangian local dynamics than the SCM. Interestingly, the lognormal model also provides a good approximation to the N-body simulations, irrespective of the nature of the initial spectra and the smoothing scales. Apparently, this contradicts with the perturbation results which predict the strong spectral dependence in weakly non-linear regime (Bernardeau 1994b). As stated by Bernardeau (1994a) and Bernardeau & Kofman (1995), however, the perturbation results themselves resemble the lognormal PDF near the index $n = -1$. Further, a systematic comparison with lognormal prediction done by Kayo, Taruya & Suto (2001), who basically used the same N-body data as ours, shows that the lognormal model prediction tends to deviate from simulation for $n = 0, +1$ in the weakly non-linear regime even if the cutoff of the PDF is taken into account. Thus, no serious contradiction is found at least at the quality of our data.

Now, consider the cumulants of the density fields. Figures 6 and 7 show the variance, the skewness and the kurtosis, which are compared with the prediction from the SCM and the ECM, respectively. As anticipated from figure 5, the amplitude of the cumulants from N-body data are significantly reduced and the prediction from local approximation without cutoff (*open-squares*) generally overpredicts the simulation results. A more serious aspect is that the simulation does not converge to the tree-level results of perturbation theory. Even the predictions up to the one-loop correction overpredict the simulation results. As previously remarked by Colombi, Bouchet & Hernquist (1996), the recovery of tree-level results is difficult for the limited size of N-body simulations and a care must be taken in order to correct the spurious numerical effects. Colombi, Bouchet & Hernquist (1996) devised to correct the finite volume effect to explore the scaling properties of the PDFs. Nevertheless, the general tendency between our simulations and those obtained by Colombi, Bouchet & Hernquist (1996) is quite similar, i.e., the non-linear correction to the skewness and the kurtosis seen in the N-body results is generally small and their amplitudes are nearly constant on scales.

In figures 6 and 7, repeating the same procedure as in the Λ CDM case, we plot the cumulant predictions from the PDF taking account of the cutoff: *open-triangles* (cutoff-1) and *filled-triangles* (cutoff-2). Then, the overall behaviors of the model predictions seem to be greatly improved. The agreement between the model prediction and the N-body simulation is reasonably good in both cutoff-1 and cutoff-2 cases except for the strongly non-linear regime, $\sigma_l \gtrsim 5$. A closer look at these figures shows that the prediction based on the ECM provides a better approximation than that of the SCM especially for the $n = 0$ case. Note, however, that most of the prediction for the variance slightly overpredict the simulation except for the $n = -2$ case. The overprediction might be partially ascribed to the cutoff of the density $[\delta_{\min}, \delta_{\max}]$, since the the width of the PDF quantified by the variance sensitively depends

on the cutoff. On the other hand, the reduced amplitudes S_3 and S_4 rather characterize the shape of the PDF, which could be, in principle, less sensitive to the cutoff of the high-density tails than cumulants themselves if the tails of PDF converges to zero enough. Actually, the shape of the predicted PDF resembles that of the PDF in the simulations as in figure 5. The same tendency has been previously reported by Fosalba & Gaztañaga (1998a).

Thus, at a level of the quality of N-body data, the local approximation with both the SCM and the ECM works reasonably well and the approximation with ECM even slightly improves the prediction. Of course, one must still care about the cutoff density arising from the spurious numerical effects. In this respect, the validity of the local approximation may just reach at an acceptable level. In addition, another important caveat is drawn from the strong model dependence of the predictions. As discussed in section 3.3, the local approximation itself becomes more sensitive to the choice of the Lagrangian local dynamics as the deviation from the spectral index $n = -3$ gets larger. This is clearly seen in the strong model dependence of the one-point PDF (Fig. 5) and the non-linear correction for the cumulant prediction (Fig. 1). Further recall the fact that the linear variance σ_l scales as $\sigma_l \propto R^{-(n+3)/2}$. This means that slight decrease of the smoothing radius R significantly increases the linear variance on non-linear scales, $\sigma_l \gtrsim 1$. Hence, one expects that the model prediction for $n \geq 0$ suffers from the non-linear corrections more seriously, compared to the initial spectra $n = -2, -1$ or Λ CDM. Therefore, the local approximation with ECM should be used with caution for the index $n \geq 0$.

5. Conclusion and discussion

In the present paper, we critically examined the validity and the usefulness of the local approximation to the PDF and the cumulant predictions. Adopting the ellipsoidal and the spherical collapse model as representative model of the Lagrangian local dynamics, the PDFs and the cumulants are calculated taking account of the smoothing effect and the resultant predictions are compared with the N-body simulations with a Gaussian initial condition. Due to the cutoff of the density arising from the spurious numerical effects, the detailed comparison in cumulants becomes difficult, and the correction for the cutoff density should be self-consistently incorporated into the model prediction. At a level of the quality of the N-body data, however, the local approximation with both SCM and ECM successfully reproduces the N-body results for the PDFs and the cumulants, although a self-consistent calculation of local approximation presented in this paper (labeled by “cutoff-2”) is still needed to be improved. This is indeed the case of the Λ CDM model and the scale-free models with indices $n = -2, -1$. For the scale-free model with $n = 0$, while the discrepancy between the

model prediction and the simulation result is manifest in the local approximation with SCM, the agreement with N-body results still remains good for the ECM prediction. The detailed discussion reveals that the prediction based on the local approximation sensitively depends on the slope of the initial spectrum and that the predictions for $n > 0$ become more sensitive to the non-linear dynamics of the local collapse model. Thus, a more delicate modeling of the Lagrangian local dynamics is required for an accurate prediction. Taking this point carefully, we therefore conclude that the local approximation with SCM and ECM provides an excellent approximation to the N-body simulations for CDM and scale-free models with $n < 0$ in both the linear and the non-linear regimes, $0 \lesssim \sigma_l \lesssim 5$, while the local approximation should be used with caution in the $n \geq 0$ cases.

In this paper, we found that the predictions based on the ellipsoidal collapse model somewhat improve the approximation, however, the degree of the improvement is not so large as long as a CDM-like initial spectrum (i.e., effective spectral index $n_{\text{eff}} = -3 - d \log \sigma_l^2 / d \log R < 0$) is concerned. Compared to the prediction from the spherical collapse model, the calculation of PDF from ellipsoidal collapse model is rather complicated and require a time-consuming numerical integration. It seems that the spherical collapse model provides a simpler prescription for the PDF in real space and is practically more useful than the ellipsoidal collapse model. However, if one considers the one-point statistics in redshift space, the situation might be changed drastically. As reported by Scherrer & Gaztañaga (2001), the local approximation with spherical collapse model only provides a good approximation to the redshift space PDFs when $\sigma_l \lesssim 0.4$. A part of this reason is ascribed to the fact that the model prediction cannot recover the linear perturbation result, referred to as the Kaiser effect (Kaiser 1987); the variance in the redshift space, σ_z^2 is related to the one in the real space as:

$$\sigma_z^2 = \left(1 + \frac{2}{3} f_\Omega + \frac{1}{5} f_\Omega^2 \right) \sigma_l^2. \quad (92)$$

In contrast to the spherical collapse model, which leads to the incorrect prediction $\sigma_z^2 = (1 + f_\Omega/3)^2 \sigma_l^2$, the Kaiser effect (92) can be correctly recovered by means of the ellipsoidal collapse model. The derivation of equation (92) is presented in appendix A. This fact is very interesting and also provides an important suggestion that the non-sphericity of the Lagrangian local dynamics play a crucial role in computing the one-point statistics in redshift space and is indeed essential for an accurate prediction. The detailed analysis of the model predictions in redshift space is now in progress and will be described elsewhere.

We thank the referee, E. Gaztañaga for many useful comments and suggestions to improve the original manuscript. We also thank Y. P. Jing for kindly providing us his N-body data and Y. Suto for comments and discussions. I.K. acknowledges support from a

Takenaka-Ikueikai Fellowship. This work is supported in part by a Grant-in-Aid for Scientific Research from the JSPS(No.14740157).

A. Derivation of Kaiser factor by ellipsoidal collapse model

In this appendix, we derive the Kaiser effect (92) from the ellipsoidal collapse model. Assuming the distant-observer approximation, let us consider the local density located at $\mathbf{r} = (r_1, r_2, r_3)$ in real space and choose the third axis as the line-of-sight direction. Denoting the corresponding coordinate in the redshift space by $\mathbf{s} = (s_1, s_2, s_3)$, the relation \mathbf{r} and \mathbf{s} becomes

$$s_1 = r_1, \quad s_2 = r_2, \quad s_3 = r_3 + v_3/H, \quad (\text{A1})$$

where v_3 is the line-of-sight component of the peculiar velocity field. Then the local density in redshift space, ρ_s can be expressed in terms of the quantities in real space as follows:

$$\rho_s = \frac{dM}{ds_1 ds_2 ds_3} = \frac{dM}{dr_1 dr_2 dr_3 \left(1 + \frac{1}{H} \frac{\partial v_3}{\partial r_3}\right)} = \frac{\rho}{1 + \frac{1}{H} \frac{\partial v_3}{\partial r_3}}. \quad (\text{A2})$$

The peculiar velocity field at the position \mathbf{r} is described by the motion of the homogeneous ellipsoid. Introducing the new coordinate along the principal axis of ellipsoid, $\mathbf{r}' = (r'_1, r'_2, r'_3)$, the peculiar velocity \mathbf{v} is given by

$$v_i = \bar{v}_i + \left(\frac{\dot{\alpha}_i}{\alpha_i} - H\right) r'_i \quad (\text{A3})$$

in the new coordinate system. Here, \bar{v}_i is the bulk velocity of the ellipsoid. The new coordinate \mathbf{r}' does not necessarily coincides with the original one \mathbf{r} . Rather, it is related to the original coordinate through the Euler angle, i.e., $\mathbf{r}' = R_3(\psi)R_2(\theta)R_3(\phi)\mathbf{r}$, where R_i is the rotational matrix with respect to the i -axis. Using this fact, the quantity (A3) is transformed into the original frame and we obtain

$$\begin{aligned} \frac{\partial v_3}{\partial r_3} &= \sum_{i=1}^3 [R_3(\psi)R_2(\theta)R_3(\phi)]_{3i}^{-1} \left(\frac{\dot{\alpha}_i}{\alpha_i} - H\right) [R_3(\psi)R_2(\theta)R_3(\phi)]_{i3} \\ &= \left(\frac{\dot{\alpha}_1}{\alpha_1} - H\right) \cos^2 \psi \sin^2 \theta + \left(\frac{\dot{\alpha}_2}{\alpha_2} - H\right) \sin^2 \psi \sin^2 \theta + \left(\frac{\dot{\alpha}_3}{\alpha_3} - H\right) \cos^2 \theta. \end{aligned} \quad (\text{A4})$$

Here, we neglect the bulk velocity. Substituting the above equation into (A2) yields

$$1 + \delta_s = \frac{1 + \delta}{\frac{1}{H} \left(\frac{\dot{\alpha}_1}{\alpha_1} \cos^2 \psi \sin^2 \theta + \frac{\dot{\alpha}_2}{\alpha_2} \sin^2 \psi \sin^2 \theta + \frac{\dot{\alpha}_3}{\alpha_3} \cos^2 \theta\right)}, \quad (\text{A5})$$

with the quantity δ_s being the density fluctuation in redshift space. Note that the expression is exact under the distant-observer limit. In the linear perturbation, the quantity α_i in (A5) is replaced with $a(1 - \lambda_i)$ (eq.[19]). We have

$$\delta_s = \delta_l + f_\Omega (\lambda_1 \cos^2 \psi \sin^2 \theta + \lambda_2 \sin^2 \psi \sin^2 \theta + \lambda_3 \cos^2 \theta), \quad (\text{A6})$$

where $f_\Omega \equiv d \ln D / d \ln a \simeq \Omega_m^{0.6}$. Hence, the linear variance in redshift space, σ_z^2 is expressed as

$$\sigma_z^2 \equiv \langle \delta_s^2 \rangle = \left(1 + \frac{2}{3} f_\Omega \right) \langle (\lambda_1 + \lambda_2 + \lambda_3)^2 \rangle + \frac{1}{15} f_\Omega^2 \langle 3(\lambda_1^2 + \lambda_2^2 + \lambda_3^2) + 2(\lambda_1 \lambda_2 + \lambda_2 \lambda_3 + \lambda_3 \lambda_1) \rangle, \quad (\text{A7})$$

where we have taken the averages over the angles, ψ , θ and ϕ . Finally, the ensemble averages over the variable λ_i are taken with a knowledge of the distribution function (21):

$$\sigma_z^2 = \left(1 + \frac{2}{3} f_\Omega + \frac{1}{5} f_\Omega^2 \right) \sigma_l^2. \quad (\text{A8})$$

This is exactly the Kaiser effect. Note that in the cases adopting the spherical collapse model, the variable λ_i means $\delta_l/3$. Hence, the ensemble average over δ_l in equation (A7) immediately yields incorrect prediction, $\sigma_z^2 = (1 + f_\Omega/3)^2 \sigma_l^2$.

REFERENCES

- Bernardeau, F. 1992, ApJ, 392, 1
- Bernardeau, F. 1994a, A&A, 291, 697
- Bernardeau, F. 1994b, ApJ433, 1
- Bernardeau, F., & Kofman, L. 1995, ApJ, 443, 479
- Bond, J. R., & Myers, S.T. 1996, ApJS, 103, 1
- Coles, P., & Jones, B. 1991, MNRAS248, 1
- Coles, P., Melott, A. L., & Shandarin, S. F. 1993, MNRAS, 260, 765
- Colombi, S., Bouchet, F. R., & Hernquist, L. 1996, ApJ, 465, 14
- Doroshkevich, A. G. 1970, Astrofizika, 6, 581
- Fosalba, P., & Gaztañaga, E. 1998a, MNRAS, 301, 503
- Fosalba, P., & Gaztañaga, E. 1998b, MNRAS, 301, 535
- Gaztañaga, E., & Yokoyama, J. 1993, ApJ, 403, 450
- Hamilton, A. J. S. 1985, ApJ, 292, L35
- Jing, Y. P. 1998, ApJ, 503, L9
- Jing, Y. P., & Suto, Y. 1998, ApJ, 494, L5
- Kaiser, N. 1987, MNRAS, 227, 1
- Kayo, I., Taruya, A., & Suto, Y. 2001, ApJ, 561, 22
- Nakamura, T. T., & Suto, Y. 1995, ApJ, 447, 65
- Ohta, Y., Kayo, I., & Taruya, A. 2003 ApJ, 589, 1
- Saslaw, W. C., & Hamilton, A. J. S. 1984 ApJ, 276, 13
- Scherrer, R. J., & Gaztañaga, E. 2001, MNRAS, 328, 257
- Scoccimarro, R. 1997, ApJ, 487, 1
- Scoccimarro, R., & Frieman, J. A. 1996, ApJ, 473, 620

Taruya, A., Hamana, T., & Kayo, I. 2003, ApJ, 339, 495

Taylor, A. N., & Watts, P. I. R., 2000, MNRAS, 314, 92

Ueda, H., & Yokoyama, J. 1996, MNRAS280, 754

Table 1. Coefficients of perturbative correction for the cumulants of the density field

n	non-linear external tide				linear external tide			
	-3	-2	-1	0	-3	-2	-1	0
$s_{2,4}$	1.79	0.772	0.363	0.566	1.73	0.708	0.299	0.501
$s_{2,6}$	4.52	0.539	0.0364	0.360	4.20	0.442	-0.0202	0.165
$s_{2,8}$	14.8	0.294	-7.50×10^{-4}	0.158	13.3	0.199	-0.0113	-0.235
$S_{3,2}$	10.2	3.19	0.525	0.00379	10.2	3.19	0.587	0.130
$S_{3,4}$	53.2	4.20	-0.0169	0.0646	51.7	3.98	0.0119	0.246
$S_{4,2}$	271	63.2	6.67	-0.0227	269	63.1	7.32	0.651
$S_{4,4}$	2.19×10^3	146	0.614	0.364	2.14×10^3	141	1.16	1.41

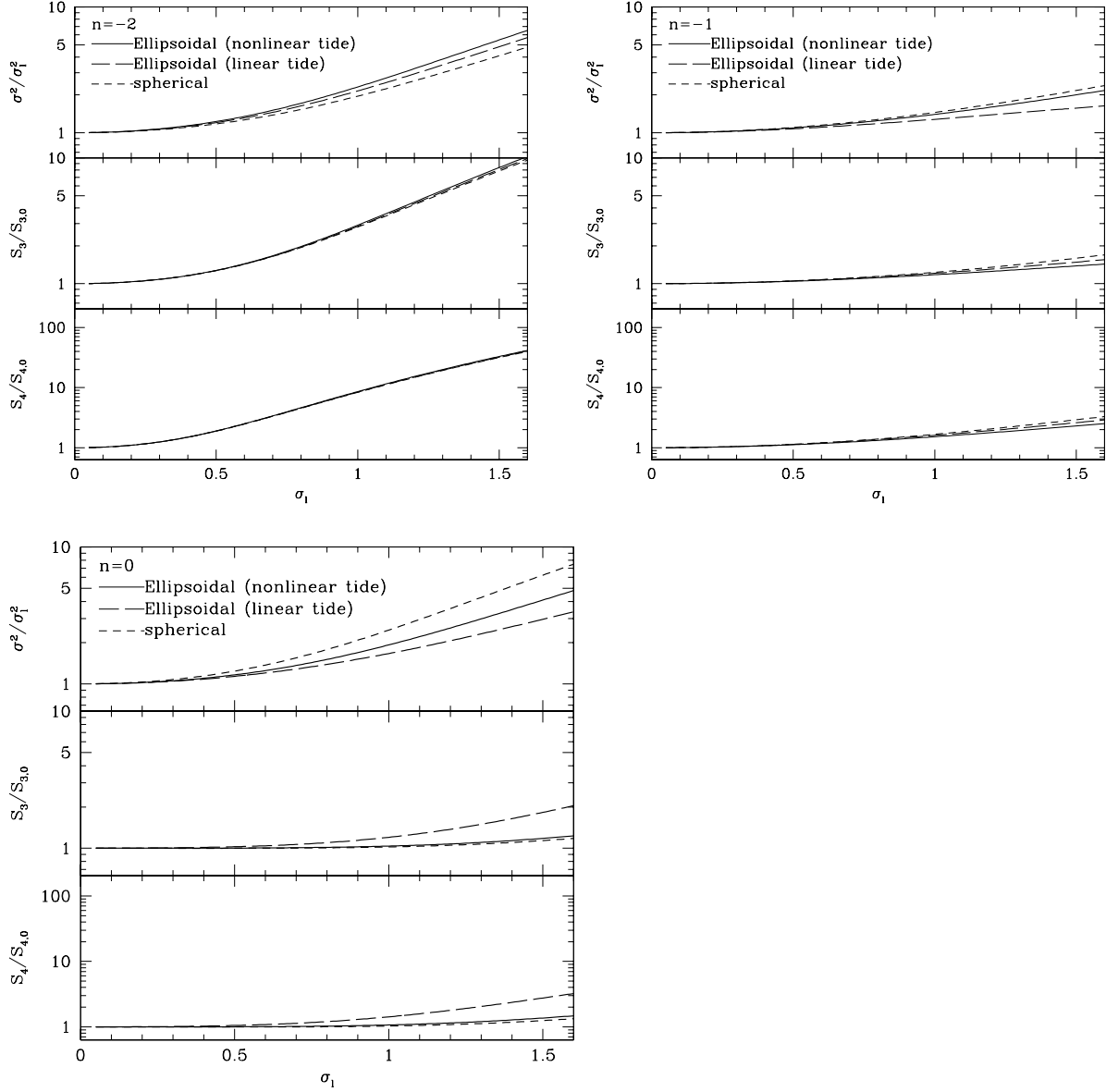


Fig. 1.— Differences between the model predictions in the variance, the skewness and the kurtosis. The perturbative results up to the two-loop order are shown in various models of the Lagrangian local dynamics. While the *solid* (*long-dashed*) lines represent the predictions based on the ECM with non-linear (linear) external tide, the *short-dashed* lines indicate the results obtained from the SCM (Fosalba & Gaztañaga 1998a).

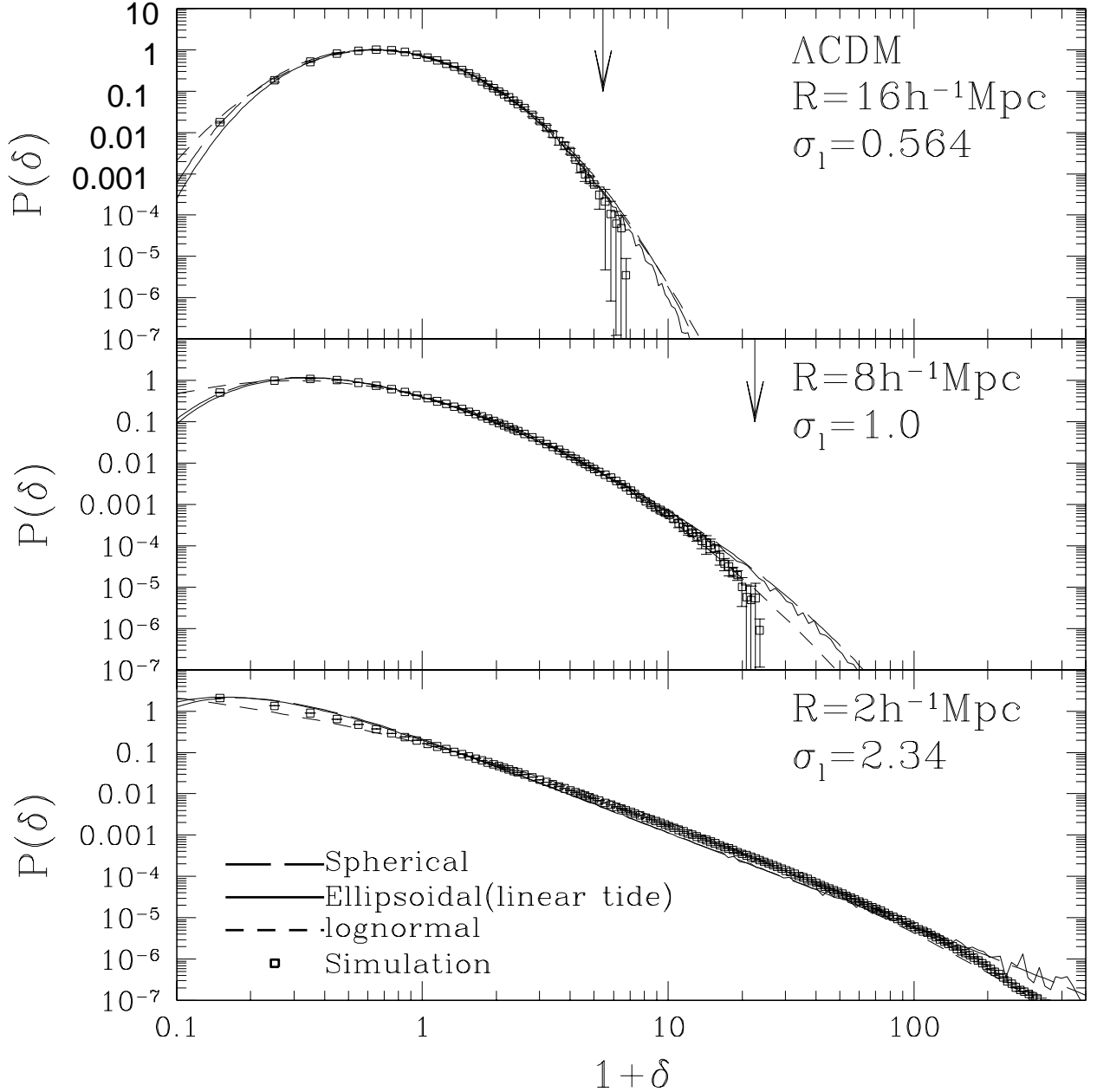


Fig. 2.— PDFs of density field in Λ CDM model with top-hat smoothing window; $R = 2$ (bottom), 8 (middle) and $16h^{-1}\text{Mpc}$ (top). The *open-squares* represent the N-body results. The error bars indicate the 1σ variation among three different realizations. Values of σ_l in each panel are the linear variance at each smoothing radius. The arrows indicate the mean value of the cutoff density δ_{max} . Note that the cutoff density at $R = 2h^{-1}\text{Mpc}$ reaches at 601. *Solid lines*: the prediction based on the ECM with linear external tide. *Long-dashed lines*: the prediction obtained from the SCM. *Short-dashed lines*: the lognormal PDF adopting the variance σ^2 calculated directly from the simulations.

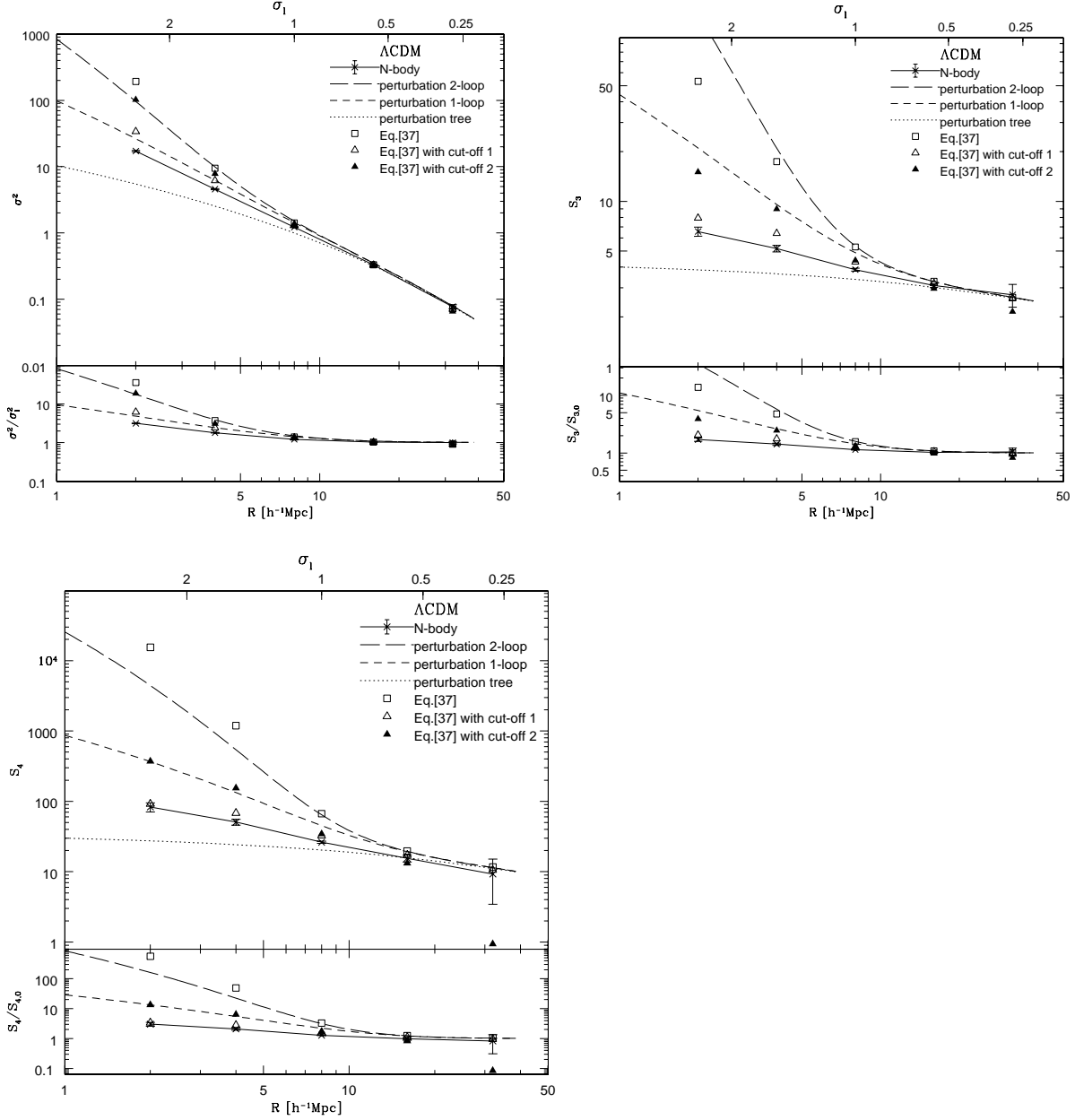


Fig. 3.— Variance (*top*), skewness (*middle*) and kurtosis (*bottom*) of the density field in ΛCDM model as function of smoothing radius R . The *crosses* with error bars represent the results from N-body simulations. The *open-squares* show the prediction from the ECM with linear external tide based on a full knowledge of the PDF (eq.[37]). The *open- and filled-triangles* are the same prediction as *open-squares*, but taking account of the limited range of the density PDF, $[\delta_{\min}, \delta_{\max}]$ (cutoff-1, cutoff-2). While the cutoff values in *open-squares* are estimated from the N-body data, δ_{\min} and δ_{\max} in *filled-triangles* are determined from equation (91) with a help of theoretical PDF. *Long-dashed* lines: the perturbative predictions of cumulants based on the ECM up to the two-loop order. *Short-dashed* lines: the perturbative predictions up to the one-loop order. *Dotted* lines: the leading order results of the perturbation theory.

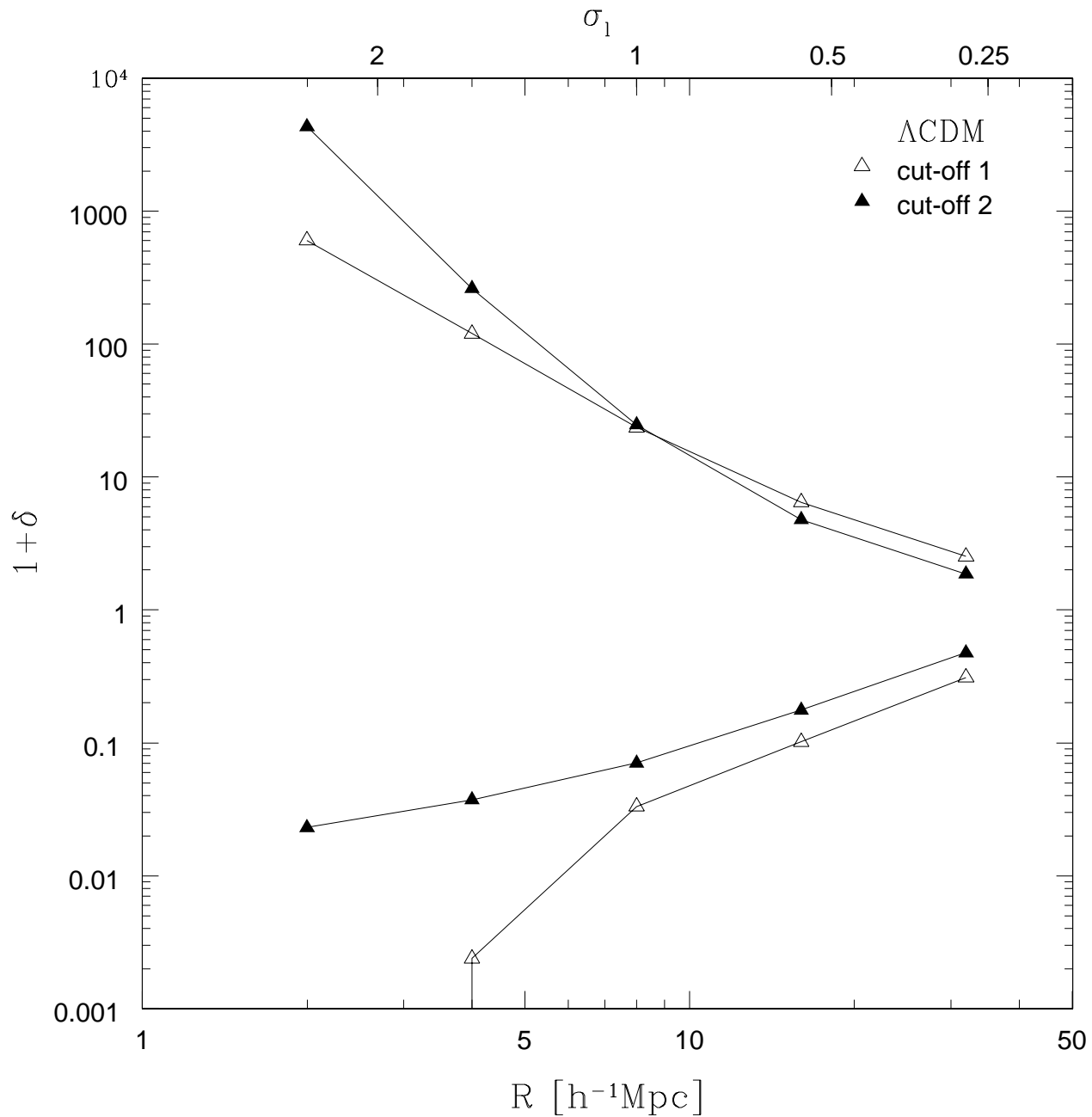


Fig. 4.— The cutoff values of the density field δ_{\min} and δ_{\max} as function of smoothing radii. While the *open-triangles* show the cutoff density estimated from the N-body simulations, the *filled-triangles* represent the values obtained from the finite sampling effect (91).

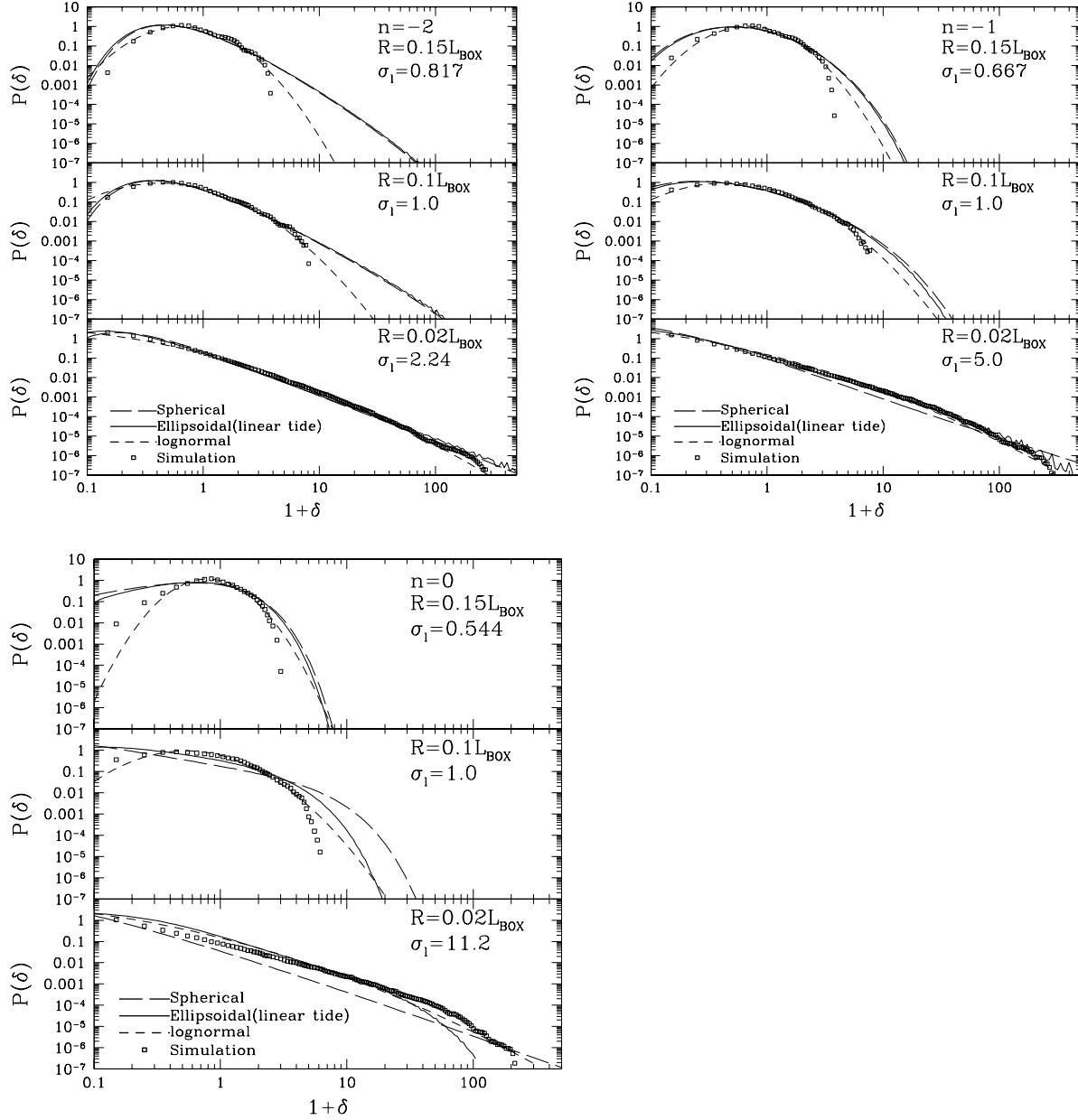


Fig. 5.— Same as Fig.2, but in the scale-free models ($n = -2, -1, 0$); $R = 0.02$ (bottom), 0.05 (middle) and $0.15L_{\text{BOX}}$ (top).

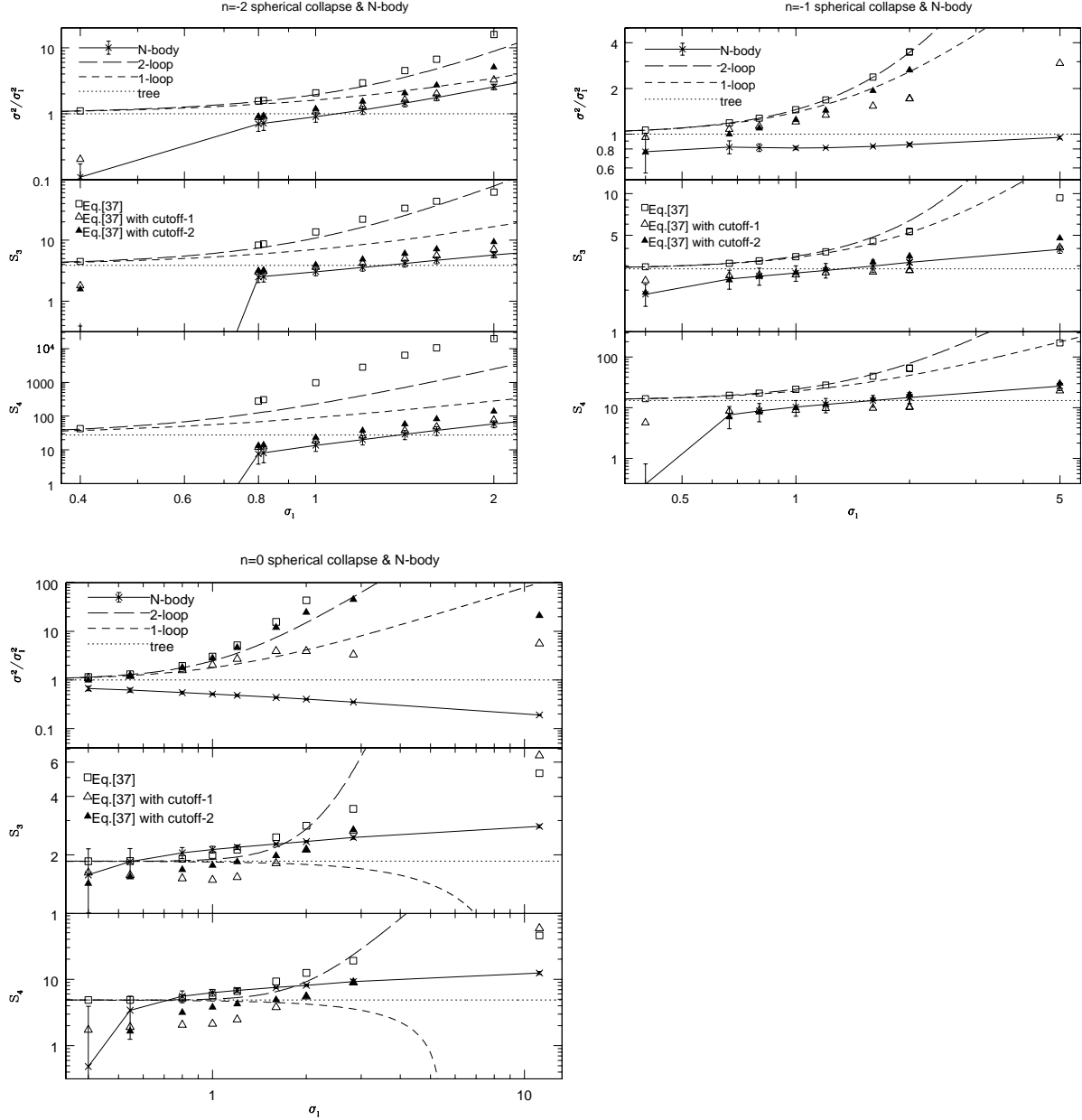


Fig. 6.— The variance, the skewness and the kurtosis of the N-body results in scale-free models, compared with the SCM predictions. The *crosses* with error bars and *solid* line represent the N-body simulations. The *squares* show the predictions from the SCM based on a full knowledge of the PDF (eq.[37]). The *open-, filled-triangles* are the same as *squares*, but we take account of the cutoff of the density field (cutoff-1, cutoff-2). While the *long-dashed* lines represent the perturbative predictions up to the two-loop order, the *short-dashed* lines indicate the results up to the one-loop order. As a reference, we also plot the leading-order results of perturbation theory in *dotted* line.

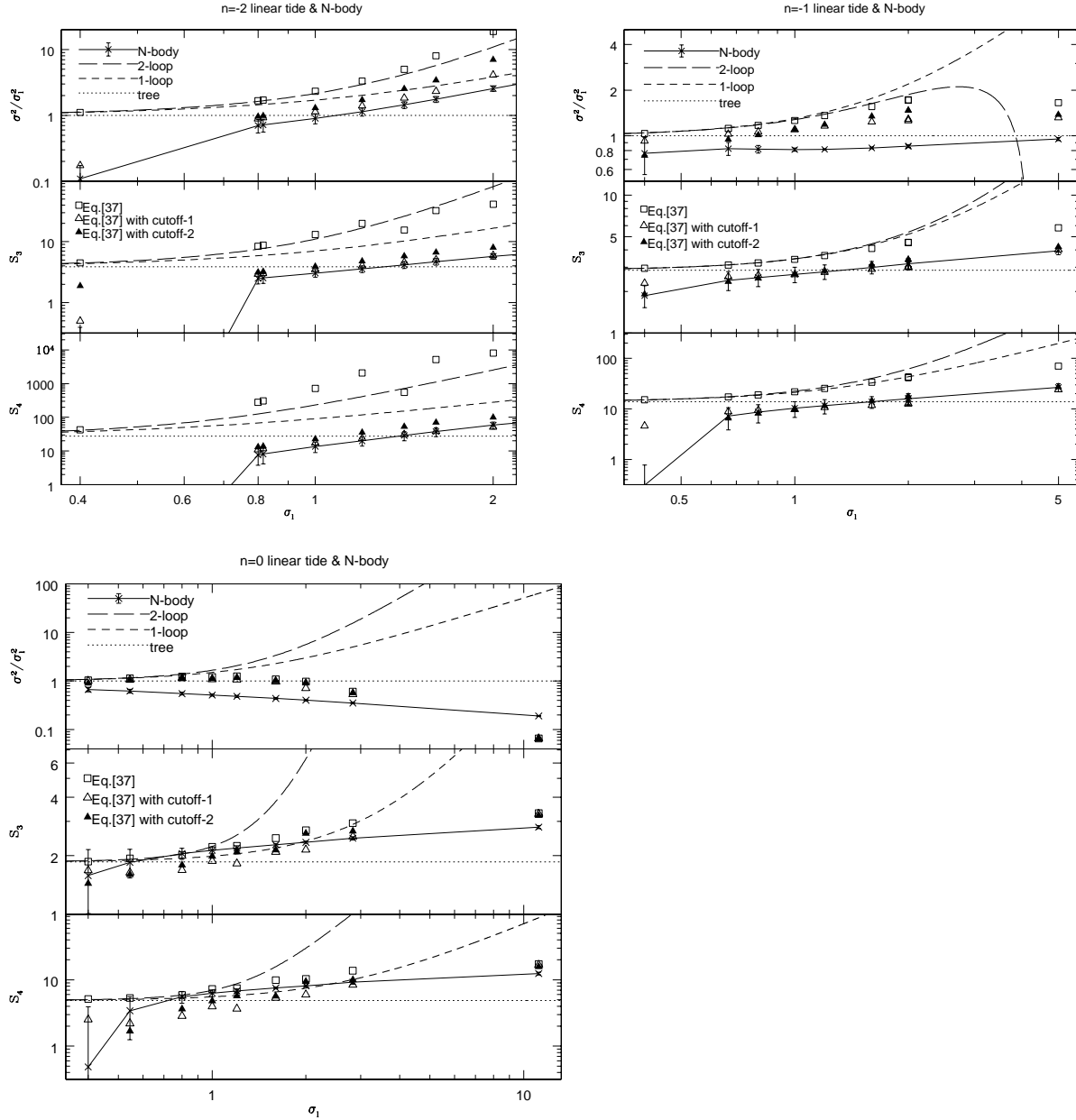


Fig. 7.— Same as figure 6, but the theoretical predictions based on the ECM with linear external tide approximation are presented.